DOI: 10.1478/AAPP.96S3A12

AAPP | Atti della Accademia Peloritana dei Pericolanti
Classe di Scienze Fisiche, Matematiche e Naturali
ISSN 1825-1242

Vol. 96, No. S3, A12 (2018)

MODELING AND STEERING MAGNETO-ELASTIC MICRO-SWIMMERS INSPIRED BY THE MOTILITY OF SPERM CELLS

MARTA ZOPPELLO [a*], ANTONIO DE SIMONE [b],
FRANÇOIS ALOUGES [c] AND LAETITIA GIRALDI [d]

ABSTRACT. Controlling artificial devices that mimic the motion of real microorganisms, is attracting increasing interest, both from the mathematical point of view and applications. A model for a magnetically driven slender micro-swimmer, mimicking a sperm cell is presented, supported by two examples showing how to steer it. Using the Resistive Force Theory (RTF) approach [J. Gray and J. Hancock, J. Exp. Biol. 32, 802 (1955)] to describe the hydrodynamic forces, the micro-swimmer can be described by a driftless affine control system where the control is an external magnetic field. Moreover we discuss through at first an asymptotic analysis and then by numerical simulations how to realize different kinds of paths.

1. Introduction

In the last decade, micro-motility has been attracting growing interest, both for the biological understanding of micro-organisms and technological applications. In the latter direction, the topic addresses several challenges as for instance the conception of artificial self-propelled and/or easily controllable microscopic robots. Such kind of devices could revolutionize the biomedical applications (Peyer *et al.* 2013) as for instance it could be useful to minimize invasive microsurgical operations (Nelson *et al.* 2010).

Learning skills from biological organisms requires, in particular, that we learn how to move and control continuously deformable objects such as filaments, cilia, and flagella. This is, in fact, an instance of bio-inspired soft robotics, where novel designs are inspired by the study of how animals exploit soft materials to move effectively in complex and unpredictable natural environment. There exists now a quite wide literature that makes a connection between the problem of swimming at the micro-scale, and the mathematical control theory. Starting from the pioneering work of Shapere and Wilczek (1989) and Montgomery (2002), the dynamics of self-propelled microscopic artificial swimmers has been considered for instance in Alouges *et al.* (2008, 2013), Alouges and Giraldi (2013), Gérard-Varet and Giraldi (2015), and Giraldi *et al.* (2015) where the rate of shape changes of the swimmer is considered as a natural control.

The aim of the present paper is to study the mechanism of propulsion of two examples of magneto-elastic artificial micro-swimmers: the first one is a swimmer, that we call "magneto-elastic Purcell swimmer", composed by only 3 links which are supposed to be uniformly magnetized and linked together with rotational springs. The second one, inspired by the work of Dreyfus (Dreyfus *et al.* 2005) consists of a swimmer that looks like a sperm cell, with a head and a tail made of a film of permanent magnetic material, and activated by an external magnetic field. At first we briefly recall a general model for magneto-elastic swimmers, following Alouges *et al.* (2015). Then regarding the Purcell Magneto-elastic swimmer, by an asymptotic analysis, we prove that it is possible to steer it along a chosen direction when the control functions are prescribed as an oscillating external magnetic field. For the sperm-like magneto-elastic micro-swimmer, we show that by actuating it with a magnetic field composed of a constant longitudinal component and an oscillatory transversal one, one can propel it along the longitudinal axis. Moreover this longitudinal magnetic field can be used as a steering device, and by varying its direction one can guide the magneto-elastic swimmer along curved trajectories and even bends of sharply curved pipes.

2. Formulation of the problem

Following Alouges *et al.* (2013, 2015), we think of our swimmer as composed by N segments, which move in the plane $z = 0$.

This two-dimensional setting is suitable for the study of slender, essentially one-dimensional swimmers exploring planar trajectories as explained in Alouges *et al.* (2013, 2015). The swimmer consists of N rigid segments, each of length L with articulated joints at their ends. We define by (x,y) the coordinates of the first end of the first link and we call θ the angle that the first segment makes with the horizontal x-axis and α_i, for $i = 1,\cdots,N-1$, the relative angle between the $i+1$ and the i-th segment (see Figure 1). The N segments are uniformly magnetized with magnetization $\mathbf{M}_i$ and linked together with torsional springs, with elastic constant K, that tend to align the segments one with another. Those produce torques when the segments are not fully aligned. In what follows we assume that an external magnetic field $\mathbf{H}(t) := \begin{pmatrix} H_x(t) \\ H_y(t) \\ 0 \end{pmatrix}$ is applied and that it is horizontal in such a way that the motion holds in the horizontal plane. For the $i-$th segment, the torques due to the external field and to the torsional springs take the form

$$\begin{aligned} \mathbf{T}_i^m &= \mathbf{M}_i \times \mathbf{H} \\ \mathbf{T}_{i,\mathbf{x}_i}^{el} &= K\alpha_i \mathbf{e}_z \end{aligned} \tag{1}$$

2.1. Equations of motion. As it was noticed in Alouges *et al.* (2015) the equations which govern the dynamics of the swimmer form a system of ODEs, which is affine with respect to the magnetic field $\mathbf{H}(t)$. The hydrodynamic forces acting on the i-th link, are approximated by using Resistive Force Theory (RTF) introduced in Gray and Hancock (1955), according to which the forces exerted by the fluid on the swimmer are linear in its velocity. We will denote the parallel (resp. perpendicular) drag coefficients with ξ_i (resp. η_i). In our particular case this system describes the evolution of position and shape variables and thus consists of

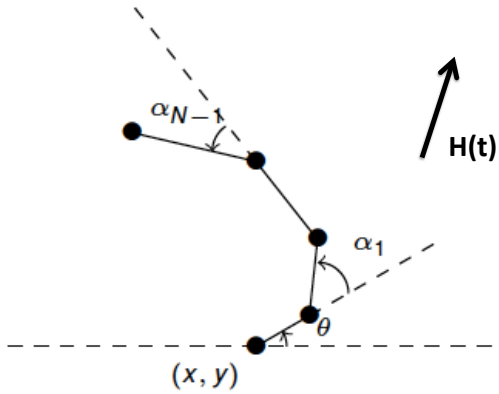

FIGURE 1. The magneto-elastic N-link swimmer.

$N+2$ equations. Those are obtained by writing the balance of forces for the whole swimmer and the balance of torques for the subsystems consisting of the N, $N-1\cdots 1$ rightmost segments. We call those subsystems $S_1, S_2, \cdots S_N$ respectively (S_1 is therefore the whole system). The motion of the swimmer holds in the horizontal plane since only horizontal forces and vertical torques apply. The final system reads:

$$\begin{cases} \mathbf{F}_h = 0\,, \\ \mathbf{e}_z \cdot \left(\mathbf{T}_h^{S_1} + \mathbf{T}_e^{S_1} + \mathbf{T}_m^{S_1}\right) = 0\,, \\ \mathbf{e}_z \cdot \left(\mathbf{T}_h^{S_2} + \mathbf{T}_e^{S_2} + \mathbf{T}_m^{S_2}\right) = 0\,, \\ \vdots \\ \mathbf{e}_z \cdot \left(\mathbf{T}_h^{S_N} + \mathbf{T}_e^{S_N} + \mathbf{T}_m^{S_N}\right) = 0\,. \end{cases} \tag{2}$$

Here, $\mathbf{F}_h$ denotes the total hydrodynamic force acting on the swimmer, $\mathbf{T}_h^{S_i}$ (resp. $\mathbf{T}_e^{S_i}$ and $\mathbf{T}_m^{S_i}$) is the hydrodynamic (resp. elastic and magnetic) torque of the subsystem S_i.

Following the construction made in Alouges *et al.* (2015) system (2) becomes

$$\mathbf{M}_h(\theta,\alpha)\begin{pmatrix} \dot{\mathbf{x}} \\ \dot{\theta} \\ \dot{\alpha}_1 \\ \vdots \\ \dot{\alpha}_{N-1} \end{pmatrix} = -K\begin{pmatrix} 0 \\ 0 \\ 0 \\ \alpha_1 \\ \vdots \\ \alpha_{N-1} \end{pmatrix} - \mathbf{M}_m^x(\theta,\alpha)H_x(t) - \mathbf{M}_m^y(\theta,\alpha)H_y(t)\,, \tag{3}$$

with $\mathbf{M}_h$ $(N+2)\times(N+2)$ matrix, $\mathbf{M}_m^x$ and $\mathbf{M}_m^y$ vectors in $\mathbb{R}^{N+2}$ all depending on $(\theta,\alpha) := (\theta,\alpha_1,\cdots,\alpha_{N-1})$. All these matrices can be computed explicitly following the approach given in Alouges *et al.* (2015).

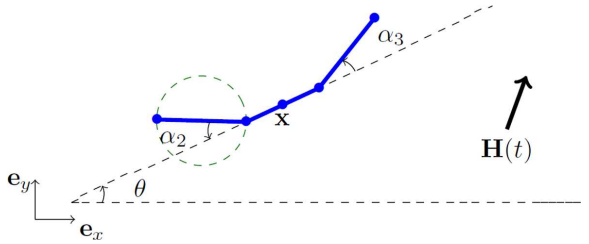

FIGURE 2. The magneto-elastic Purcell swimmer of shape (α_2, α_3) at the position $\mathbf{x}$ in the plane subject to an external magnetic field $\mathbf{H}$.

3. Two cases study

In this section we will analyse two examples, the first one is a generalization of the well known Purcell three link swimmer, that we call Purcell magneto-elastic swimmer, and a second example of a swimmer composed by 10 segments which try to move mimicking a sperm cell. For the first example by an asymptotic analysis, we prove that it is possible to steer the swimmer along a chosen direction when using an oscillating external magnetic field. In the second example, using values for the geometric and material parameters which are realistic for a magnetic multi-layer, we discuss the possibility to make the swimmer moving straight or to steer the system along curved paths.

3.1. Purcell magneto-elastic swimmer. To benefit from the symmetry of the system, for this particular system we use as state variables the coordinate $\mathbf{x} := (x, y)$ of the middle point of the second segment, and the angle θ that it forms with the x-axis. With the notation of the preceding section, we call α_2 and α_3 the relative angles to the central link of the left and right arms respectively, see Figure 2. To compute the equation of motion we follow the same procedure described in the preceeding section considering all the links equally magnetized. In this way from (3) we end up with

$$\begin{pmatrix} \dot{\mathbf{x}} \\ \dot{\theta} \\ \dot{\alpha}_2 \\ \dot{\alpha}_3 \end{pmatrix} = \mathbf{f}_0(\theta, \alpha_2, \alpha_3) + \mathbf{f}_x(\theta, \alpha_2, \alpha_3) H_x(t) + \mathbf{f}_y(\theta, \alpha_2, \alpha_3) H_y(t) \tag{4}$$

We can solve for $\dot{\mathbf{x}}$ as

$$\dot{\mathbf{x}} \quad = \mathbf{G}_1(\theta, \alpha_2, \alpha_3)\, \dot{\theta} + \mathbf{G}_2(\theta, \alpha_2, \alpha_3)\, \dot{\alpha_2} + \mathbf{G}_3(\theta, \alpha_2, \alpha_3)\, \dot{\alpha_3}\,. \tag{5}$$

Regarding instead the subsystem associated with the shape and the orientation of the swimmer we have

$$\begin{pmatrix} \dot{\theta} \\ \dot{\alpha}_2 \\ \dot{\alpha}_3 \end{pmatrix} = \mathbf{g}_0(\theta, \alpha_2, \alpha_3) + \mathbf{g}_x(\theta, \alpha_2, \alpha_3) H_x(t) + \mathbf{g}_y(\theta, \alpha_2, \alpha_N) H_y(t)\,. \tag{6}$$

In order to overcome any symmetry obstruction (Alouges *et al.* 2017) we assume that our Purcell magneto-elastic swimmer satisfies

$$\eta_2 = \eta_3 = \eta \quad \xi_2 = \xi_3 = \xi \qquad \text{with } \eta_1 \neq \eta \quad \xi_1 \neq \xi \tag{7}$$

They are suitable for example in the case of a swimmer with an head.
Starting from a swimmer with a horizontal shape ($\theta = \alpha_2 = \alpha_3 = 0$), we can use the horizontal component of the external magnetic field as a "stabilizer" whereas the oscillating vertical component produces the shape deformation and the motion. In order to understand further what happens when such a field is applied we make the following perturbation analysis. We assume that

$$(H_x(t), H_y(t)) = (1, \varepsilon \sin(\omega t)), \tag{8}$$

and compute the asymptotic expansion of the swimmer displacement with respect to small ε after a period $\frac{2\pi}{\omega}$.

Linearizing the system of equations (6) for small angles $(\tilde{\theta}, \tilde{\alpha}_2, \tilde{\alpha}_3)$, to first order in ε we get that the triplet $\begin{pmatrix} \tilde{\theta} \\ \tilde{\alpha}_2 \\ \tilde{\alpha}_3 \end{pmatrix}$ satisfies the equation,

$$\begin{pmatrix} \dot{\tilde{\theta}} \\ \dot{\tilde{\alpha}}_2 \\ \dot{\tilde{\alpha}}_3 \end{pmatrix} = \mathbf{A} \begin{pmatrix} \tilde{\theta} \\ \tilde{\alpha}_2 \\ \tilde{\alpha}_3 \end{pmatrix} + b \sin(\omega t) \tag{9}$$

with

$$\mathbf{A} = \nabla (\mathbf{g}_0 + \mathbf{g}_x)(0,0,0)\ ,\ b = \mathbf{g}_y(0,0,0)\,. \tag{10}$$

Here, $\mathbf{A}$ is the 3×3 matrix which depends on the drag coefficients, (η_1, η) and (ξ_1, ξ), on the magnetization M and on the elastic constant K.

The solution of the system (9) is thus given by

$$\begin{pmatrix} \tilde{\theta}(t) \\ \tilde{\alpha}_2(t) \\ \tilde{\alpha}_3(t) \end{pmatrix} = \frac{1}{2i} \left(\mathbf{A}^+(\omega) \exp(i\omega t) b - \mathbf{A}^-(\omega) \exp(-i\omega t) b \right) + \mathbf{c}(\omega) \exp(\mathbf{A}t) \tag{11}$$

where $\mathbf{A}^{\pm}(\omega) := (-\mathbf{A} \pm i\omega \mathbf{I})^{-1}$ and $\mathbf{c}(\omega) = \mathbf{A}^-(\omega) b - \mathbf{A}^+(\omega) b$.
The first part of the solution is a periodic solution, while the last is an exponentially decaying perturbation, as we shall see now. Indeed, by applying Routh-Hurwitz criterion on the characteristic polynomial of $\mathbf{A}$, we prove that the real part of its eigenvalues are all negative. This provides the stability of the asymptotic periodic solution.

Proposition 3.1. *The steady-state solution, called $\mathscr{S}^\infty$, of* (9)

$$\mathscr{S}^\infty(t) = \frac{1}{2i} \left(\mathbf{A}^+(\omega) \exp(i\omega t) b - \mathbf{A}^-(\omega) \exp(-i\omega t) b \right), \tag{12}$$

is stable.

Proof: The characteristic polynomial of $\mathbf{A}$ reads

$$p_{\mathbf{A}}(\lambda) = \det(\mathbf{A} - \lambda \mathbf{Id}) = a_3 \lambda^3 + a_2 \lambda^2 + a_1 \lambda + a_0\,,$$

where

$$a_0 = \det\mathbf{A} = -\frac{432M\left(3K^2+4KM+M^2\right)(2\eta+\eta_1)}{d} < 0,$$

$$a_1 = -\frac{36}{d}\left(M^2\left(10\eta^2+28\eta\eta_1+\eta_1^2\right)+K^2\left(16\eta^2+64\eta\eta_1+\eta_1^2\right)+KM\left(31\eta^2+98\eta\eta_1+3\eta_1^2\right)\right) < 0,$$

$$a_2 = \mathrm{tr}\mathbf{A} = \frac{-12}{d}\left(M\left(2\eta^2+17\eta\eta_1+5\eta_1^2\right)+K\left(2\eta^2+37\eta\eta_1+9\eta_1^2\right)\right) < 0,$$

$$a_3 = -1 < 0$$

$$d = L^9\eta^2\left(8\eta\eta_1+7\eta_1^2\right)$$

and

$$a_3a_0 - a_2a_1 = \frac{-1}{L^9\eta^3\eta_1^2(8\eta+7\eta_1)^2}\Big(432\big(2(K+M)(16K^3+31KM+10M^2)\eta^4+$$
$$+5\left(144K^3+339K^2M+217KM^2+42M^3\right)\eta^3\eta_1+\left(2514K^3+5015K^2M+2867KM^2+506M^3\right)\eta^2\eta_1^2+$$
$$+\left(613K^3+1309K^2M+802KM^2+150M^3\right)\eta\eta_1^3+(9K+5M)\left(K^2+3KM+M^2\right)\big)\eta_1^4\Big) < 0.$$

Using the Routh-Hurwitz criterion (Gantmacher 1959), we have that the real part of the eigenvalues of $\mathbf{A}$ is negative and therefore the steady state of the equation (9) is stable. □

As a consequence, the solution of (11) exponentially converges to the periodic solution (12) and in particular $\theta \sim \varepsilon\tilde{\theta}^\infty$ oscillates around 0 indicating that the swimmer stays nearly horizontal, stabilized by the horizontal component of the magnetic field. Similarly, the fact that the shape variables (α_2,α_3) are periodic (and small) indicates that the swimmer stays nearly straight.

In order to go further, and compute the (asymptotic) net displacement of the swimmer after one period of the oscillating external field, we linearize as well the equation (5) in $(\theta,\alpha_2,\alpha_3)$ near $(0,0,0)$.

Noting,

$$\dot{x} = \mathbf{G}^x(\theta,\alpha_2,\alpha_3)\cdot\begin{pmatrix}\dot\theta\\ \dot\alpha_2\\ \dot\alpha_3\end{pmatrix} \quad \text{and} \quad \dot{y} = \mathbf{G}^y(\theta,\alpha_2,\alpha_3)\cdot\begin{pmatrix}\dot\theta\\ \dot\alpha_2\\ \dot\alpha_3\end{pmatrix}$$

where $\mathbf{G}^x$ (resp. $\mathbf{G}^y$) is the 1×3 matrix composed of $(\mathbf{G}_i\cdot\mathbf{e}_x)_{i=1,\cdots 3}$ (resp. $(\mathbf{G}_i\cdot\mathbf{e}_y)_{i=1,\cdots 3}$), we obtain Δx as

$$\int_0^{\frac{2\pi}{\omega}} \varepsilon\left(\mathbf{G}^x(0,0,0)+\varepsilon^t\mathscr{S}^\infty(t')\nabla\mathbf{G}^x(0,0,0)\right)\mathscr{S}^\infty(t')\mathrm{d}t' + o(\varepsilon^2).$$

Since, $t\mapsto\mathscr{S}^\infty(t)$ is periodic, the latter equality reads

$$\Delta x = \varepsilon^2\int_0^{\frac{2\pi}{\omega}} {}^t\mathscr{S}^\infty(t')\nabla\mathbf{G}^x(0,0,0)\mathscr{S}^\infty(t')\mathrm{d}t' + o(\varepsilon^2), \tag{13}$$

and a straightforward computation leads to express

$$\nabla \mathbf{G}^x(0,0,0) = \frac{L}{2(2\eta+\eta_1)} \begin{pmatrix} 2(\eta-\eta_1) & -\eta_1 & \eta \\ -\frac{(6\eta\eta_1-4\eta\xi+\eta_1\xi_1}{(2\xi+\xi_1)} & -\frac{\eta_1(2\eta+\xi_1)}{(2\xi+\xi_1)} & -\frac{\eta(\eta_1-\xi_1)}{(2\xi+\xi_1)} \\ \frac{(2\eta^2+4\eta\eta_1-3\eta_1\xi)}{(2\xi+\xi_1)} & \frac{\eta_1(\eta-\xi)}{(2\xi+\xi_1)} & \frac{\eta(\eta+\eta_1+\xi)}{(2\xi+\xi_1)} \end{pmatrix}.$$

Similarly, the same formula holds for Δy by substituting $\mathbf{G}^x$ with $\mathbf{G}^y$ and in this case,

$$\nabla \mathbf{G}^y(0,0,0) = \begin{pmatrix} 0 & 0 & 0 \\ 0 & 0 & 0 \\ 0 & 0 & 0 \end{pmatrix},$$

thus, $\Delta y = o(\varepsilon^2)$. It follows that the leading term, with respect to small angles, of the trajectory of the swimmer along the y-axis is negligible after one period of the oscillating fields compared to the one along the x-axis.

From now on, we focus on the x-displacement of the swimmer, Δx and we prove that the leading term of order ε^2 does not vanish after one period of the oscillating fields.

Plugging (12) into (13) and noting that the two terms vanish because of periodicity,

$$\int_0^{\frac{2\pi}{\omega}} t \left(\mathbf{A}^+(\omega)\exp(i\omega t)b\right) \nabla \mathbf{G}^x(0,0,0) \left(\mathbf{A}^+(\omega)\exp(i\omega t)b\right) = 0,$$
$$\int_0^{\frac{2\pi}{\omega}} t \left(\mathbf{A}^-(\omega)\exp(-i\omega t)b\right) \nabla \mathbf{G}^x(0,0,0) \left(\mathbf{A}^-(\omega)\exp(-i\omega t)b\right) = 0$$

we obtain Δx as

$$\Delta x = \varepsilon^2 \int_0^{\frac{2\pi}{\omega}} \frac{\omega}{4} \left({}^t b\, {}^t\mathbf{A}^+(\omega)\mathbf{N}\mathbf{A}^-(\omega)b\right), \tag{14}$$

where $\mathbf{N}$ is the 3×3 matrix $(\nabla \mathbf{G}^x(0,0,0) - {}^t\nabla \mathbf{G}^x(0,0,0))$.

Moreover, the 3×3 matrix $\mathbf{N}$ is skew-symmetric and not null. Therefore, 0 is an eigenvalue of multiplicity 1. Let us denote by $\mathbf{u}$ its associated eigenvector. A direct computation leads to

$$\mathbf{u} = \begin{pmatrix} \eta_1\xi + \eta\xi_1 - 2\eta\eta_1 \\ 2\eta^2 + 4\eta_1\eta - 2\xi\eta - \xi_1\eta - 3\eta_1\xi \\ 6\eta\eta_1 - 2\xi\eta_1 - 4\eta\xi_1 \end{pmatrix}.$$

Thus, to ensure that (14) is not null, it is sufficient to prove that the triple of vectors $\{\mathbf{u}, \mathbf{A}^-(\omega)b, \mathbf{A}^+(\omega)b\}$ are independent. But, for large frequencies ω, we can expand the matrix $\mathbf{A}^\pm(\omega)$ as

$$\mathbf{A}^\pm(\omega) = \pm\frac{\mathbf{I}}{i\omega} - \frac{\mathbf{A}}{\omega^2} + o(\frac{1}{\omega^2}). \tag{15}$$

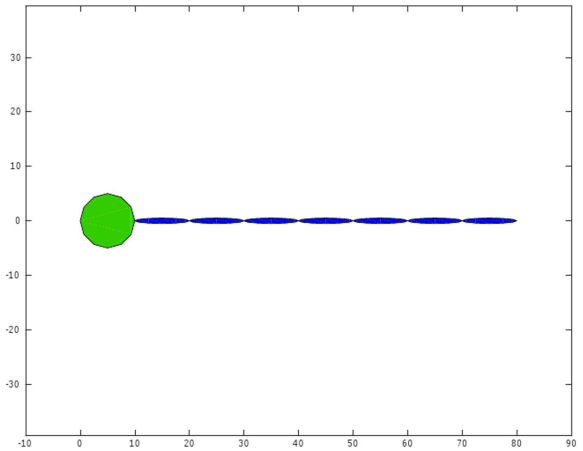

FIGURE 3. The magneto-elastic swimmer: initial configuration, before the application of the external magnetic field.

and

$$\det(\mathbf{u}, \mathbf{A}^-(\omega)b, \mathbf{A}^+(\omega)b) = \det(\mathbf{u}, \frac{\mathbf{b}}{\omega}, \frac{\mathbf{Ab}}{\omega^2}) + o(\frac{1}{w^4}) =$$
$$-\left(L^9\omega^3\eta^3\eta_1^2(8\eta+7\eta_1)^2(3\eta\eta_1-2\eta\xi_1-\eta_1\xi)\right)^{-1}\times$$
$$\times\Big(\eta\eta_1(113K+38M)+216M^2(2\eta+\eta_1)\big(\eta^2\xi_1\big(4\eta^2(5K+2M)+\eta_1^2(29K+8M)\big)$$
$$+\eta\eta_1(\eta_1-\eta)\big(K\left(4\eta^2+37\eta\eta_1+13\eta_1^2\right)+6\eta_1M(2\eta+\eta_1)\big)-\eta_1\xi\big(8\eta^3(2K+M)$$
$$+2\eta^2\eta_1(40K+13M)+\eta\eta_1^2(53K+14M)+\eta_1^3(13K+6M)\big)\Big)\Big).$$

This determinant does not vanish identically then we obtain that by prescribing an oscillating magnetic field as (8), the magneto-elastic Purcell swimmer moves along the x-axis. Notice that here the assumption on the drag coefficients (7) is crucial.

3.2. Moving mimicking sperm cells. Let us now consider the swimmer depicted in Figure 3, which consists of a large (say, disk-shaped) head linked to a tail composed of 10 segments. Each segment, including the head, is $10\mu m$ long, so that the length of the whole system is $110\,\mu m$. In order to represent a continuous tail made of a Permalloy thin film, we use the following values for the magneto-elastic parameters: $K = \frac{1}{12}10^{-11}Nm$ and $M_s = 8\cdot10^{-8}A\,m$. As for the drag coefficients, we follow Friedrich *et al.* (2010) and take $\xi_i = 6.2\cdot10^{-3}$ Nsm^{-2}, $\eta_i = 12.4\cdot10^{-3}\,Nsm^{-2}$, for $i = 2,\cdots,N$, $\xi_1 = \eta_1 = 0.05Nsm^{-2}$.

3.2.1. *Straight swimming.* We first consider the case where the swimmer, originally in the horizontal position, is excited by a magnetic field similar to the one used in the previous

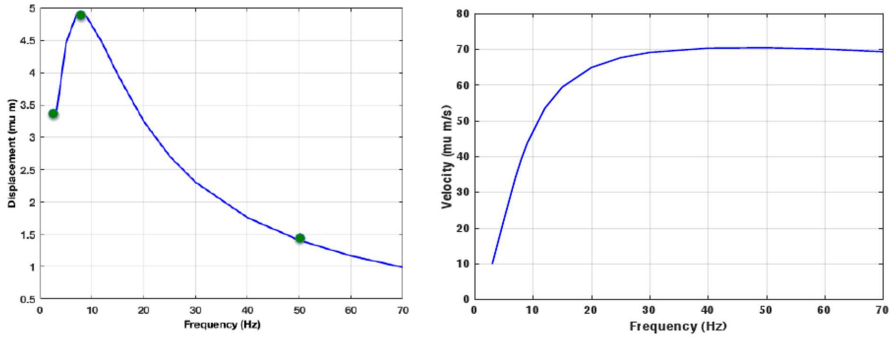

FIGURE 4. Horizontal displacement during one period of the external field (left) and velocity of the swimmer (right). Very small and very high frequencies are not effective and a maximum displacement is obtained for a frequency of about 8 Hz. Three bullets indicate the frequencies 3, 8 and 50 Hz that are used in the sequel for a more thorough analysis.

example, with a constant horizontal component and an oscillating vertical one

$$\mathbf{H}(t) = (H_x, H_y \sin(\omega t))^t \tag{16}$$

where $H_x = 0.01\,T$ and $H_y = 0.02\,T$ are fixed. These values have been selected on a trial-and-error basis, as field strengths of magnitude achievable in a laboratory and producing interesting performance. Notice that the presence of a nonzero value of H_x proved necessary to obtain stable net motion along the horizontal axis.

We explore the dynamics of the swimmer by varying the driving frequency $\omega/2\pi$ in the range 3-70 Hz. We see from Figure 4 that the net horizontal displacement per cycle is maximised at about 8 Hz, while the maximal swimming speed is attained around 50 Hz. The value of this maximal displacement is close to 5 μm, while the maximal swimming speed is around 70μm/s. The evolving shape of the swimmer is well characterised by the angle $\Psi(s,t)$ between the horizontal axis and the tangent to the swimmer at arc-length distance s from the external end of the head segment. Following Friedrich *et al.* (2010), we compute the Fourier coefficients of $\Psi(s,\cdot)$

$$\widehat{\Psi}_n(s) = \int_0^{\frac{2\pi}{\omega}} \Psi(s,t) \exp(in\omega t)\, dt$$

From a numerical analysis of $\dfrac{\widehat{\Psi}_1(s)\overline{\widehat{\Psi}_1(0)}}{|\widehat{\Psi}_1(0)|}$ [performed as in Alouges *et al.* (2015)] it can be shown that $\widehat{\Psi}_1(s)$ is well approximated by a function of the type $\widehat{\Psi}_1(s) = \lambda + \mu s \exp(i\varphi)$ which indicates a behaviour of $\Psi(s,t)$ that is well approximated by the function

$$\Psi(s,t) \sim Re(\widehat{\Psi}_1(s)\exp(i\omega t)) \sim \lambda\cos(\omega t) + \mu s \cos(\omega t + \varphi)\,. \tag{17}$$

The deformation of the swimmer is thus composed of a global rotation (the spatially constant term) and of a term describing bending with a spatially constant curvature (the term linear

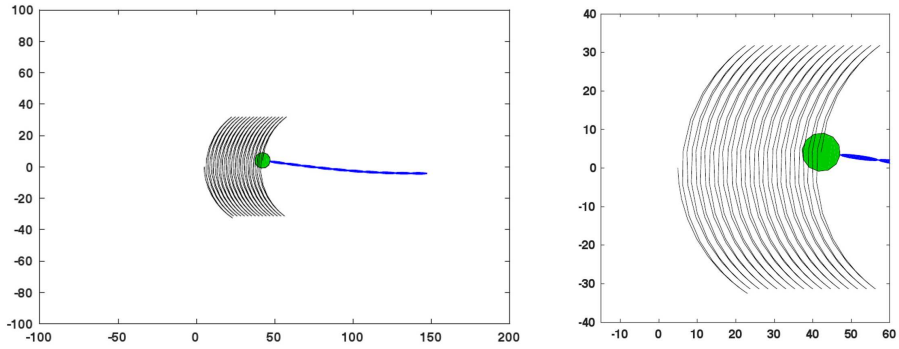

FIGURE 5. Trajectory of the head of the swimmer with the magnetic field given by (16) with $\omega = 8$ Hz. The close-up view in the right panel emphasizes the oscillations in the head movement. Lengths are in μm.

in s), which both oscillate in time with angular frequency ω and a phase shift φ. According to (17), there is no travelling wave of curvature propagating along the tail of the swimmer. Therefore, this swimming mechanism is very different from the one observed in sperm cells in Friedrich *et al.* (2010), but also from the one observed in the artificial system described in Dreyfus *et al.* (2005), which is also actuated by an external oscillating magnetic field. In particular, notice that by differentiating (17) with respect to s, we obtain that the curvature remains constant along the tail of the swimmer (i.e., s-independent) at every time, while being modulated by a time-dependent amplitude (see Figure 5).

3.2.2. *Swimming in circles.* The previous section shows that, as it was pointed out already in Dreyfus *et al.* (2005), the constant horizontal component of the magnetic field (which is parallel to the initial straight configuration of the magnetic tail, and then parallel to its average orientation during the motion), acts in a stabilising way, keeping the average orientation of the swimmer always aligned with it. Indeed, the swimmer oscillates, following the oscillations of the transversal component of the applied field, but its average motion is that of a translation along the average direction of the oscillating magnetic field, which is horizontal.

If we now consider an external magnetic field which is obtained by superposing fast transversal oscillations with frequency ω on a slowly varying longitudinal field, oscillating at frequency $\omega' \ll \omega$, we expect that we can use the direction of the slowly varying field to steer the swimmer. As an example, consider an external magnetic field of the form

$$\mathbf{H} = H_{\parallel}\mathbf{e}_{\theta(t)} + H_{\perp}\sin(\omega t)\mathbf{e}^{\perp}_{\theta(t)} \tag{18}$$

where $\mathbf{e}_{\theta(t)}$ is the unit vector forming an angle $\theta(t)$ with the horizontal axis given by

$$\theta(t) = 2\pi t/T_{\max}\,, \tag{19}$$

and $H_{\parallel}$ and $H_{\perp}$ have again the values of $H_x = 0.01\,T$ and $H_y = 0.02\,T$, respectively. Here, in order to have a clear separation of the time scales associated with fast and slow oscillations,

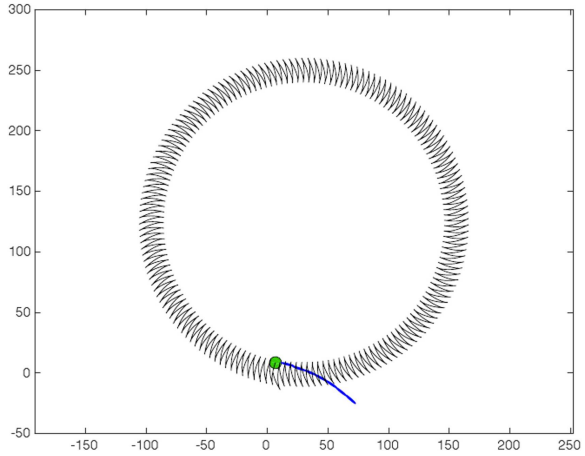

FIGURE 6. Trajectory of the head of the swimmer with the magnetic field given by equations (18, 19). The average direction of the magnetic field experiences a low frequency circular motion together with a high frequency oscillation. The swimmer follows the slow modulations of the applied magnetic field by tracing a circular trajectory. Lengths are in μm.

we take $\omega/2\pi = 8\,\text{Hz}$, and $T_{\max} = 40\,s$, which, in view of (19) leads to a frequency $\omega'/2\pi = 0.025\,Hz \ll \omega/2\pi$.

The swimmer traces now a circular trajectory, and its average orientation follows the slow modulations of the applied magnetic field (see Figure 6).

3.2.3. *Turning abruptly.* In this last section we push further the idea developed in the previous section. Indeed, we take the same parameters as before, and use now a magnetic field given by (18) which oscillates around an average orientation $\mathbf{e}_{\theta(t)}$ that now varies in time according to

$$\theta(t) = \frac{\pi}{4}\left(1 + \tanh\left(30\left(\frac{t}{T_{\max}} - \frac{1}{2}\right)\right)\right). \tag{20}$$

Notice that $\theta(t)$ experiences a sudden jump from 0 to $\frac{\pi}{2}$ around $t = \frac{T_{\max}}{2}$. The result we obtain is displayed in Figure 7 and shows clearly a sudden change in the swimming direction which would allow the swimmer to navigate along an elbow in a pipe. Here, we are tacitly assuming that the pipe is wide enough with respect to the size of the swimmer so that the hydrodynamics effects of the walls can be neglected. Enriching the model to consider explicitly the confining effects due to the pipe walls would be interesting, also in view of recent results in Alouges and Giraldi (2013), but will not be done here.

4. Conclusions

In this paper we analyzed two examples of magneto-elastic microswimmers, one inspired by the well known classical Purcell swimmer and the other one that resembles a sperm cell. In both cases we show that by prescribing a particular oscillating magnetic field we are able to steer the swimmer along one direction, at first by an asymptotic analysis on a

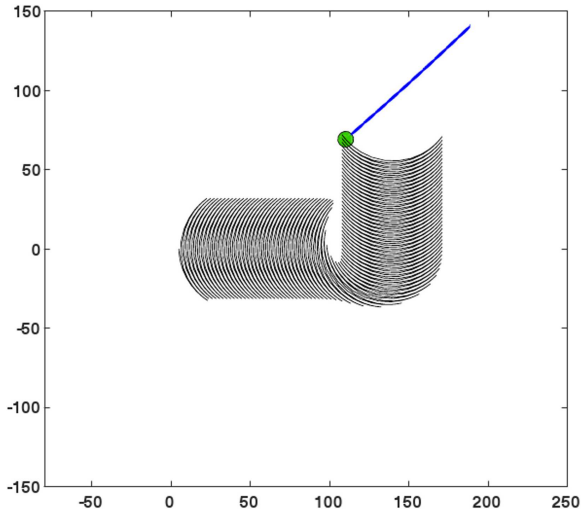

FIGURE 7. Trajectory of the head of the swimmer with the magnetic field given by equations (18, 20) where we have used $\omega/2\pi = 8$ Hz and $T_{\max} = 10s$. The sudden rotation of the axis along which the magnetic field oscillates induces a sudden change in the swimming direction that could allow the swimmer to navigate along the elbow of a pipe (not shown). Lengths are in μm.

"toy model" swimmer and then by numerical simulations which use geometric parameters consistent with those achievable by current manufacturing techniques,. Our analysis provide a feasibility study for the engineering of microscopic artificial swimmers. We showed that our magneto-elastic swimmer propels itself with a mechanism, which is very different from the ones previously reported in the literature for flexible magneto-elastic filaments. Indeed, the deformation of the swimmer is composed of a global rotation and of a bending deformation with a spatially constant curvature, which both oscillate in time at the same frequency of the external magnetic field, but with a phase shift. By contrast, sperm cells and artificial swimmers exploiting control of their curvature propel themselves by propagating internally activated waves of bending along the flagellum.

References

Alouges, F., DeSimone, A., Giraldi, L., and Zoppello, M. (2013). "Self-propulsion of slender micro-swimmers by curvature control: N-link swimmers". *Journal of Non-Linear Mechanics* **56**, 132–141. DOI: 10.1016/j.ijnonlinmec.2013.04.012.

Alouges, F., DeSimone, A., Giraldi, L., and Zoppello, M. (2015). "Can magnetic multilayers propel micro-swimmers mimicking sperm cells?" *Soft Robotics* **2**(3), 117–128. DOI: 10.1089/soro.2015.0007.

Alouges, F., DeSimone, A., Giraldi, L., and Zoppello, M. (2017). *Purcell Magneto-Elastic Swimmer Controlled by an External Magnetic Field*. 20th IFAC Coference Toulouse.

Alouges, F., DeSimone, A., and Lefebvre, A. (2008). "Optimal strokes for low Reynolds number swimmers : an example". *Journal of Nonlinear Science* **18**(3), 277–302. DOI: 10.1007/s00332-007-9013-7.

Alouges, F. and Giraldi, L. (2013). "Enhanced controllability of low Reynolds number swimmers in the presence of a wall". *Acta Applicandae Mathematicae* **128**(1), 153–179. DOI: 10.1007/s10440-013-9824-5.

Dreyfus, R., Baudry, J., Roper, M. L., Fermigier, M., Stone, H. A., and Bibette, J. (2005). "Microscopic artificial swimmers". *Nature* **437**, 862–865. DOI: 10.1038/nature04090.

Friedrich, B. M., Riedel-Kruse, I. H., Howard, J., and Jülicher, F. (2010). "High-precision tracking of sperm swimming fine structure provides strong test of resistive force theory". *Journal of Experimental Biology* **213**(8), 1226–1234. DOI: 10.1242/jeb.039800.

Gantmacher, F. R. (1959). *Applications of the Theory of Matrices*. New York: Wiley, DOI: 10.1137/1006054.

Gérard-Varet, D. and Giraldi, L. (2015). "Rough wall effect on microswimmer". *ESAIM: COCV* **21**(3), 757. DOI: 10.1051/cocv/2014046.

Giraldi, L., Martinon, P., and Zoppello, M. (2015). "Optimal Design for the three-link Purcell swimmer". *Physical Review E* **91**, 023012. DOI: 10.1103/PhysRevE.91.023012.

Gray, J. and Hancock, J. (1955). "The propulsion of sea-urchin spermatozoa". *Journal of Experimental Biology* **32**(4), 802–814. DOI: jeb.biologists.org/content/32/4/802.

Montgomery, R. (2002). *A tour of subriemannian geometries, theirs geodesics and applications*. American Mathematical Society. DOI: http://dx.doi.org/10.1090/surv/091.

Nelson, B. J., Kaliakatsos, I. K., and Abbott, J. J. (2010). "Microrobots for minimally invasive medicine". *Annu. Rev. Biomed. Eng.* **12**(15), 55–85. DOI: 10.1146/annurev-bioeng-010510-103409..

Peyer, K. E., Zhang, L., and Nelson, B. J. (2013). "Bio-inspired magnetic swimming microrobots for biomedical applications". *Nanoscale* **5**(4), 1259–1272. DOI: 0.1039/c2nr32554c.

Shapere, A. and Wilczek, F. (1989). "Efficiencies of self-propulsion at low Reynolds number". *J. Fluid Mech.* **198**, 587–599. DOI: 10.1017/S0022112089000261.

---

[a] Università degli Studi di Padova
Via Trieste 63, 35121 Padova Italy,

[b] Scuola Internazionale di Studi Superiori Avanzati (SISSA)
via Bonomea 265, 34136 Trieste, Italy

[c] École Polytechnique CNRS
Route de Saclay, 91128 Palaiseau France

[d] INRIA Sophia Antipolis Méditerranée
Route des Lucioles 2004, 06902 Valbonne, France

* To whom correspondence should be addressed | email: mzoppell@math.unipd.it

Paper contributed to the workshop entitled "Mathematical modeling of self-organizations in medicine, biology and ecology: from micro to macro", which was held at Giardini Naxos, Messina, Italy (18–21 September 2017) under the patronage of the *Accademia Peloritana dei Pericolanti*

Manuscript received 26 February 2018; published online 30 November 2018